



UNIVERSITY OF LEEDS

This is a repository copy of *Solubility and Nucleation of Methyl Stearate as a Function of Crystallization Environment*.

White Rose Research Online URL for this paper:
<http://eprints.whiterose.ac.uk/128034/>

Version: Accepted Version

Article:

Camacho Corzo, DM orcid.org/0000-0001-5330-4110, Roberts, KJ orcid.org/0000-0002-1070-7435, More, I et al. (1 more author) (2018) Solubility and Nucleation of Methyl Stearate as a Function of Crystallization Environment. *Energy and Fuels*, 32 (3). pp. 3447-3459. ISSN 0887-0624

<https://doi.org/10.1021/acs.energyfuels.7b03212>

(c) 2018, American Chemical Society. This document is the Accepted Manuscript version of a Published Work that appeared in final form in *Energy & Fuels*, copyright (c) American Chemical Society after peer review and technical editing by the publisher. To access the final edited and published work see: <https://doi.org/10.1021/acs.energyfuels.7b03212>

Reuse

Items deposited in White Rose Research Online are protected by copyright, with all rights reserved unless indicated otherwise. They may be downloaded and/or printed for private study, or other acts as permitted by national copyright laws. The publisher or other rights holders may allow further reproduction and re-use of the full text version. This is indicated by the licence information on the White Rose Research Online record for the item.

Takedown

If you consider content in White Rose Research Online to be in breach of UK law, please notify us by emailing eprints@whiterose.ac.uk including the URL of the record and the reason for the withdrawal request.



eprints@whiterose.ac.uk
<https://eprints.whiterose.ac.uk/>

SOLUBILITY AND NUCLEATION OF METHYL STEARATE AS A FUNCTION OF CRYSTALLISATION ENVIRONMENT

Diana M. Camacho^{a*}, Kevin J. Roberts^a, Iain More^b, Ken Lewtas^{b,c}

[a] School of Chemical and Process Engineering, University of Leeds, Leeds, LS2 9JT, UK

[b] Infineum UK Ltd, Milton Hill Business and Technology Centre, Abingdon, OX13 6BB,
UK

[c] Current address: Lewtas Science & Technologies Ltd., Oxford, OX2 7DY, UK

Keywords: Biodiesel cold-flow behaviour, solubility, solution ideality, nucleation kinetics and mechanism, methyl esters, solvent effect, solution turbidometric characterisation, polythermal method, KBHR model

*Corresponding author

To be submitted to Energy & Fuels

ABSTRACT

Crystallisation studies of methyl stearate from supersaturated dodecane, kerosene and toluene solutions reveal strong evidence that solvent choice influences solubility and nucleation behaviour. Solute solubility is less than ideal with toluene, kerosene and dodecane, respectively exhibiting the closest behaviour to ideality, the latter consistent with the highest solvation.

Polythermal crystallisation studies using the KBHR model [1-3], reveal a progressive nucleation (PN) mechanism with crystallite interfacial tension (γ_{eff}) values between 0.94-1.55, 1.21 - 1.91 and 1.18-1.88 $\frac{mJ}{m^2}$ for dodecane, kerosene and toluene, respectively. Nucleation rates at the critical undercooling lie between 4.56×10^{16} and $1.79 \times 10^{17} \frac{nuclei}{mL sec}$, with the highest rates associated with crystallisation from kerosene solutions. Iso-supersaturation nucleation rates are the highest for dodecane ranging from 2.39×10^{17} and $3.63 \times 10^{18} \frac{nuclei}{mL sec}$.

Nucleation in toluene appears to be hindered by its relatively higher interfacial tension which is associated with nucleation rates about an order of magnitude less than those obtained for dodecane.

1. Introduction

The study of diesel and biodiesel fuel crystallisation is of importance to the fuels industry as poor cold-flow properties of these mixtures can cause operability problems within vehicles engines, pipelines and vehicle tanks under cold weather conditions due to the formation of crystals at low temperatures. To date most research has focussed on the crystallisation within diesel fuel [4-15], which mostly comprises alkanes, with much less emphasis being placed to the study of biodiesel fuel. First generation of biodiesel fuels are generally a mixture of both saturated and unsaturated methyl esters from which the former represent an important proportion of these solution and commonly contain methyl palmitate (C16:0) and stearate (C18:0). The cold-flow behaviour of biodiesel is determined to a great extent by the amount of saturated compounds present in its composition.

Some studies [16-19] have been carried out in order to characterise the cold-flow behaviour of biodiesel fuel produced from different bio-resources, measuring certain properties such as: cloud point (CP), pour point (PP) and cold filter plugging point (CFPP) and the effect of cold-flow improvers on these properties. The fractionation of methyl esters crystallising from biodiesel fuel mixtures produced from different bio-resources has also been addressed [20-25]. However, up to now there has been a lack of fundamental studies on the nucleation of saturated methyl esters, such as methyl palmitate and stearate.

As a baseline case, it is the aim of this study to deliver fundamental information on the solubility and nucleation of methyl stearate measured as a function of solution environment. In this, the solubility is assessed using the van't Hoff analysis [26]. This was combined with a rigorous analysis of the associated nucleation data through the recent developed KBHR theory

[1-3]. This theory, outlined in section 2 of the paper, permits a first principle analysis of nucleation kinetics and enables the derivation of key kinetic parameters and the characterisation of the nucleation mechanism.

As in real-world operation biodiesel fuel is commonly mixed with traditional diesel fuel, three different model solvents were chosen representing the variation in solvation environment, viz. dodecane, toluene and kerosene.

2. Nucleation kinetics and mechanism

2.1. Classical nucleation theory (CNT) and its assessment

The classical 3D nucleation theory (CNT) provides a model for the prediction of the rate at which nuclei of new crystalline phase are formed. This model given by expression (1) describe the dependence of nucleation rate (J) on two terms: a thermodynamic (exponential) which accounts mainly for the effect of temperature, supersaturation ratio (S) and the effective interfacial tension (γ_{eff}) on the formation of nuclei and a “kinetic” one (pre-exponential) which described the frequency with which molecules will attach to the nucleus. The interplay of these two terms would determine a system’s nucleation behaviour.

$$J = K_J \exp \left[- \left[k_n v_o^2 \gamma_{eff}^3 / (kT)^3 (\ln S)^2 \right] \right] \quad (1)$$

Where K_J is the nucleation rate constant, k_n is the nuclei numerical shape factor i.e. $16\pi/3$ for spherical nuclei and 32 for cubic nuclei, v_o is the volume occupied by a solute molecule in the crystal, , and k is the Boltzmann constant.

$$S = \frac{x}{x_e} \quad (2)$$

Here x is the solution's molar concentration and x_e is the equilibrium concentration.

Supersaturation can also be expressed as the relative supersaturation (σ) as given by expressions (3)

$$\sigma = S - 1 \quad (3)$$

The analysis of nucleation kinetics can be performed by either the isothermal or polythermal methodologies which both use the concept of solution state metastability to create the supersaturation needed to promote nucleation. The isothermal method makes use of the kinetic expressions derived from classical nucleation theory, in particular, utilising the assumption that the induction time (τ) can be taken as being inversely related to the nucleation rate (J). In contrast the polythermal method assesses nucleation through establishing the effect of cooling rate (q) on crystallisation temperatures (T_c).

2.1.1. The isothermal method

In this method, one can calculate key nucleation parameters including the interfacial tension (γ) and the critical nucleation cluster size (r^*), as a function of solution supersaturation and temperature.

In this case, many experiments ideally should be carried out i.e. typically 5-10 different supersaturations with ca. 80 repeats at each chosen supersaturation [27]. The analysis of this

data is though relatively simple as nucleation rates can be directly extracted by fitting a probability distribution of the measured induction times. A comprehensive assessment that quantifies the uncertainty associated with the parameters estimated using this methodology is provided in the work presented by Xiao Y. et al. [28].

2.1.2. The polythermal method

The polythermal approach continuously varies the solution supersaturation, and hence induction time, upon cooling and assesses the balance between excess concentration generation via the cooling rate and the material's intrinsic nucleation rate. The effect that supersaturations has on nucleation is implicitly evaluated over the whole width of the metastable zone. This is defined, for the work presented here, as the difference between the equilibrium concentration derived from van't Hoff analysis and the solution concentration pertinent to the temperature at which spontaneous crystallisation occurs.

The process involves driving the solution by cooling until the induction time is effectively zero. i.e. the point at which spontaneous nucleation takes place. Under these conditions mass transfer due to molecular diffusion can be expected to be rapid and hence the degree of statistical variation would be much less than that for induction times measurements. The latter is typically recorded for lower supersaturations, concomitantly larger cluster sizes and lower levels of molecular diffusion.

In the polythermal case, experimental data is comparatively easy to collect using automated temperature controlled solution turbidimetric methods. As nucleation is clearly of stochastic nature, in our analysis all the determined parameters are presented with their corresponding standard deviation using the most reliable experimental methodology developed in our

previous work [3]. In this, we have shown that typically five repeats at each cooling rate are sufficient (Section 2 of the SM provided in reference [3]) to obtain reliable data to perform an assessment using this approach.

The analysis of polythermal data can be much more complex than the isothermal case and could be performed using a number of different available models, both empirical [29, 30] and first principles [31-33]. The most widely used interpretation of $\Delta T_c(q)$ data is using the empirical Nyvlt expressions [29, 30]. However, given the empirical nature of the Nyvlt approach, Kubota [31] and Sangwal [32, 33] have re-interpreted these equations in order to derive more physically meaningful parameters. An example of the application of these approaches is provided by Mitchell N.A. et al. [34] where key kinetic parameters were derived for paracetamol–ethanol solutions.

2.1.3. Comparison between isothermal and polythermal methods

Figure (1) compares the different approaches used in each of the methodologies to collect experimental data. Using a turbidimetric technique, in the isothermal method a clear homogeneous solution is rapidly cooled to a given supersaturation where the solution is kept until crystallisation is detected through the increase in the solution's turbidity, after a given induction time (τ). On the other hand, in the polythermal method a solution is cooled continuously at a given rate, until crystallisation is detected through the increase in the solution's turbidity. Although in the isothermal method the onset of crystallisation is monitored at the same temperature (or supersaturation), this method is up to a certain extent inherently polythermal as the solution has already gone through a number of different temperatures (or saturations) during the initial rapid cooling to the chosen supersaturation. Although the two

methodologies are apparently quite different, interestingly, they reach the same endpoint, e.g. as shown in Camacho D.M. et al. (Table 9 CrystEngComm, 2014) [3] nucleation parameters calculated via the two methodologies are broadly equivalent. For clarity to the reader on how to establish the corresponding supersaturations using either of the two methodologies, section 1 of the supplementary information (SI) provides also a figure in which these methods are compared based on a plot of concentration vs temperature.

Due to the nature of crystallisation in methyl esters solutions, characterised for very narrow metastable zones and very short induction times a polythermal method was used to collect experimental data. Details of this methodology are provided in section 4.

2.2. The Kashchiev-Borissova-Hammond-Roberts (KBHR) approach

A first principles analytical polythermal approach, the Kashchiev-Borissova-Hammond-Roberts (KBHR), comprises a set of model equations analytically derived starting from the Kolmogorov-Johnson-Mehl-Avrami (KJMA) expression. Such model is analogous to “chemical reaction progress kinetic analysis” [35], in which reaction progress is monitored as a function of a dynamically changing reactant concentration, which is akin to carrying out hundreds of separate initial rate experiments [35]. A key outcome of the KBHR model is the so called “rule of three” [1, 2] which can be used to discriminate between two case nucleation mechanisms, i.e.

Progressive nucleation (PN) [2] where new crystal nuclei are continuously formed in the presence of the already growing ones. In this case the measured induction times are

associated with both the nucleation and the growth processes until the crystals reach a size where they are detectable optically via the turbidimetric technique.

Instantaneous nucleation (IN) [1] where all nuclei emerge at once at the beginning of the crystallisation process to subsequently grow and develop into crystal. In this case, strong nucleation sites will favour the nucleation process and therefore inductions times are only associated with the time for these crystals to growth to a detectable size.

The expressions related to both the PN and IN mechanisms, analytically derive in the KBHR approach, are presented below [2].

2.2.1. Progressive Nucleation

The general expression relating critical undercooling and cooling rate for this mechanism is given by expression (4)

$$\ln q = \ln q_0 + a_1 \ln u_c - \frac{a_2}{(1 - u_c)u_c^2} \quad (4)$$

The relative critical undercooling (u_c) is a dimensionless quantity associated with the critical undercooling (ΔT_c) given by:

$$u_c = \frac{\Delta T_c}{T_e} \quad (5)$$

Similarly, the critical undercooling ΔT_c , which represents the solution's metastability limit in terms of temperature, is defined as:

$$\Delta T_c = T_e - T_c \quad (6)$$

where T_e and T_c are the solution equilibrium and crystallisation temperatures, respectively.

Expression (4) describes the dependence of the number of crystals at the detection point (N_{det}) on cooling rate (q) when $d = 0$ i.e. the volume of single crystals is unaccounted for (see derivation in SM), thus the free parameters a_1 , a_2 and q_0 are given by [2]

$$a_1 = 3 \quad (7)$$

$$a_2 = b \quad (8)$$

$$q_0 = \frac{VK_j T_e}{N_{det} 2b} \quad (9)$$

Where, V the volume of the solution and b is given by [2]

$$b = \frac{k_n v_o^2 \gamma_{eff}^3}{k T_e \lambda^2} \quad (10)$$

In this expression λ is the molecular latent heat of crystallisation

When equation (4) is derived by means of the relative volume of crystals (α), the parameters q_0 , a_1 and a_2 are defined by

$$a_1 = 3 + \frac{3nmd}{md + 1} \quad (11)$$

$$a_2 = \frac{b}{md + 1} \quad (12)$$

$$q_0 = T_e \left\{ \frac{\Gamma[(n + 1)md + 1] K_v \alpha^{nmd} K_J K_G^{md}}{(n + 1)^d (2b)^{(n+1)md+1} \alpha_{det}} \right\}^{\frac{1}{(md+1)}} \quad (13)$$

Here, d is the dimensionality of crystallites growth, i.e. 3 for spheres or cubes, 2 for disks or plates and 1 for needles. n and $m > 0$ are the crystallite growth exponents which are related to the different growth mechanism [36]. The $n = 1$ case corresponds to growth mediated by diffusion of solute towards the crystallite or transfer of solute across the crystal/solution interface. The $n = 2$ case characterises growth controlled by the presence of screw dislocations in the crystallite. The parameter m ranges between $\frac{1}{2}$ and 1: $m = \frac{1}{2}$ is for growth controlled by undisturbed diffusion of solute, and $m = 1$ is for growth by diffusion of solute through a stagnant layer around the crystallite or for normal or spiral growth limited by transfer of solute across the crystal/solution interface. At $m = 1$ the crystallite radius increases linearly with time [1, 2, 37]. $k_v (m^{3-d})$ is the crystallites' growth shape factor i.e. $\frac{4\pi}{3}$ for spheres, 8 for cubes, πH_0 for disks, $4H_0$ for square plates (H_0 is the fixed disk or plate thickness), and $2A_0$ for needles (A_0 is the fixed needle cross-sectional area). K_G is the crystal

growth rate constant, Γ is the gamma function and α_{det} the relative volume of crystals at the detection point

2.2.2. Instantaneous nucleation

In the case of IN the expression for the dependence of relative critical undercooling on cooling rate is given below

$$\ln q = \ln q_0 + \left(\frac{1}{m}\right) \ln \left[u_c^{(n+1)m} - u_o^{(n+1)m} \right] \quad (14)$$

In this expression $u_o \geq 0$, $u_c > u_o$ and the parameter q_0 is given by

$$q_0 = \left[\frac{k_v C_0}{(n+1)^d \alpha_{det}} \right]^{\frac{1}{m d}} a^n K_G T_e \quad (15)$$

Where C_0 is the concentration of nuclei at the time at which the instantaneous nucleated crystallites are formed and a is given by expression (16)

$$a = \frac{\lambda}{k T_e} \quad (16)$$

If additionally, the undercooling at which all nuclei spontaneously appear is small enough so that

$$u_o^{(n+1)m} \ll u_c^{(n+1)m} \quad (17)$$

Equation (14) takes the form of a straight line given by

$$\ln q = \ln q_o + (n + 1) \ln u_c \quad (18)$$

In q vs u_c line corresponding to expression (4) is only slightly curve, thus in a not too wide experimental q range it can be approximate to a straight line [1, 2]. This linear relationship can be analytically derived using an arbitrarily critical undercooling as shown in reference [2] and is given by expression (19). When comparing this expression with equation (18) then from the slope of a line of the dependence of relative critical undercooling for crystallisation (u_c) on the cooling rate (q), the nucleation mechanism can be establish using the “rule of three” [1, 2]: $slope > 3 = PN$ or $slope < 3 = IN$

$$\ln q = \ln Q + \left(3 + \frac{3nmd}{md + 1} + \omega a_2 \right) \ln u_c \quad (19)$$

In expression (19) ω is a positive number and Q is a parameter related to q_0 [1]

Both expressions (4) and (14) are subjected to the inequalities (20) as shown in the analytical derivation in section 1 of the SM. Which means that this analysis is restricted to small enough values of the critical undercooling (u) for which the inequalities are satisfied

$$u < 0.1, au < 1 \quad (20)$$

The critical radius of the nucleus (r^*) and the number (i^*) of molecules in the critical nucleus can be calculated from expressions (21) and (22) given in terms of the relative undercooling u

$$r^* = \frac{2\gamma_{eff}v_0}{\lambda u} \quad (21)$$

$$i^* = \frac{2bkT_e}{\lambda u^3} \quad (22)$$

The classical 3D nucleation rate model, given in terms of the parameters defined by the KBHR approach is presented in equation (23)

$$J(t) = K_J e^{\frac{-b}{(1-u)u^2}} \quad (23)$$

Here K_J is related to the attachment frequency of monomers to the nucleus (f^*), the concentration of nucleation sites (C_0), and the Zeldovich factor z . The latter accounts for the probability that a critical nucleus would become a crystal and not re-dissolve.

The attachment frequency (f^*) is given by either expression (24) or (25) for attachment of monomers controlled by volume diffusion or interface transfer respectively [38]

$$f^* = \xi 4\pi r^* D X_1 \quad (24)$$

$$f^* = \xi \omega^* d_0 A^* X_1 \quad (25)$$

where ξ is the sticking coefficient, D the diffusion coefficient of colliding building units, X_1 the concentration of colliding building units, ω^* the transfer frequency of building units from adsorbed to integrated, d_0 the thickness of adsorbed surface layer and A^* the surface area of nucleus.

The attachment of building units to the cluster is quite sensitive to changes in the temperature, the effect being mainly due to the viscosity. This is particularly relevant when the attachment of monomers is controlled by volume diffusion and nucleation occurs within a temperature range in which the solution viscosity varies strongly with T .

It is important to highlight here that due to the nature of the derivation of the KBHR approach, the assessment of polythermal data using this theory is subject to the following assumptions:

1. The supersaturation at which crystallisation is detected (MSZW) has to be sufficiently small, so that the solution viscosity does not change significantly within the assessed range
2. The former will allow the assumption that the nucleation mechanism does not change within the range of concentrations measured on cooling

A fuller description of this theory is provided in the SI to this paper.

3. Materials and methods

3.1. Materials

Methyl stearate, dodecane and toluene were purchased from Sigma-Aldrich. The purity of the methyl stearate used was 96% and that of the two solvents was higher than 99%. No further

purification was carried out. Kerosene was supplied by Infineum Ltd. (Milton Hill-Oxfordshire UK). Its hydrocarbon composition is summarised in Table 1. Its n-alkanes chain length distribution is given in Fig.2 of the SI.

3.2. Equipment and experimental procedure for polythermal data collection

Crystallisation experiments were carried out using the Avantium Crystal 16[®] system. This provides a multiple reactor facility with four separate Peltier heated aluminium blocks, each of which has a capacity to hold four magnetically-agitated 1 mL solution vials. Each block can be individually programmed to follow a given temperature profile during which the variations in the solution turbidity are followed as a function of temperature.

Solutions of methyl stearate in three different solvents dodecane, kerosene and toluene were prepared at solutions concentrations of 200, 250, 300 and 350 g of solute per litre of solvent for the first two solvents, and 154, 192, 231 and 269 g of solute per litre of solvent for toluene. In order to ensure accurate measurement of temperatures, calibration of the Crystal 16[®] unit was required. Four vials containing each of the solvents were placed in each of the blocks which were programmed to a specific temperature in the range of 20°C to -8°C. Whilst each block was kept at a chosen temperature, measurements of the actual temperature with $\pm 0.5^\circ\text{C}$ accuracy were carried out by positioning a thermocouple within each of the vials. The average of the four temperatures readings obtained in each block was plotted against the programmed temperature and fitted by a straight line represented by the expressions $y = 0.87x + 2.20$, $y = 0.96x + 1.34$ and $y = 0.95x + 0.99$ for dodecane, kerosene and toluene respectively. These expressions were then used to correct the experimentally measured temperature values. The temperature-calibration lines obtained are given in the SI.

The solutions were subject to heating and cooling cycles, with each cycle initiated by heating the solutions up to 40°C where they were held for 1 h to ensure complete homogenization and then cooled to -15°C where they were also held for 1 h to allow equilibration. This temperature profile was applied at each solution's concentration using four different rates 0.25, 1.0, 3.2 and 9.0 °C/min for dodecane and kerosene systems and 0.25, 0.5, 1.0 and 1.5 °C/min for toluene solutions. The range of both concentrations and cooling rates for solutions of a given solvent was chosen to ensure accurate temperature profiles. This was achieved by setting temperatures profiles in which crystallisation was detected above -15 °C (lowest working temperature of the Crystal 16[®]) and a sufficiently wide range of cooling rates in compliance with both the equipment cooling power capacity and the methodology applied. For the solutions where crystallisation was detected at lower temperatures a narrower cooling range had to be used due to the decrease in the equipment cooling capacity observed at these temperature levels.

At each rate the temperature cycle was repeated five times to obtain average values for the crystallisation and dissolution temperatures T_c and T_{diss} . These were estimated based upon the points in the turbidity profile at which sudden changes in light transmittance are detected T_c . Fig. 2 shows a typical experimental profile together with a representative raw data set for one of the experimental runs.

To assess the influence of the solute and solvent molecules polarity on the solubility of methyl stearate, its dipole moment was calculated in vacuum using three different methods: semi-empirical:AM1, Hartree-Fock:3-21G and DFT:B3LYP/6-31G* delivering values of 1.67 D, 1.54 D and 1.52 D respectively (Ken Lewtas, private communication, September 4th, 2015).

3.3. Data analysis

3.3.1. Solubility

The polythermal data were used to establish the solubility for methyl stearate in dodecane, kerosene and toluene solutions by extrapolation of the $T_{diss}(q)$ lines to 0°C/min. The solubility was modelled according to the van't Hoff equation given by expression (26). This expression is derived from the general expression of solid-liquid equilibrium assuming that specific heat capacity (ΔC_p) can be neglected. This assumption can be applied to the analysis of methyl stearate solubility as according to previous work [39] ΔC_p values does not change significant within the temperature range studied here.

$$\ln(x_e) = -\frac{\Delta H_{diss}}{RT} + \frac{\Delta S_{diss}}{R} \quad (26)$$

The strength of the solutions' chemical interactions was assessed by comparing the solubility with the ideal model solid-liquid equilibrium given by expression (27)

$$\ln(x_e) = -\frac{\Delta H_{fus}}{RT} + \frac{\Delta S_{fus}}{R} \quad (27)$$

In these expressions x_e is the mole fraction of the solute in the solution at saturation, T is the solution temperature, $\Delta H_{diss} \left(\frac{J}{mol}\right)$, $\Delta H_{fus} \left(\frac{J}{mol}\right)$ are the molal enthalpy of dissolution and fusion respectively, $\Delta S_{diss} \left(\frac{J}{mol K}\right)$, $\Delta S_{fus} \left(\frac{J}{mol K}\right)$ are the molal entropy of dissolution and fusion respectively and $R \left(8.314 \frac{J}{mol K}\right)$ is the gas constant.

A compound's molar solubility, can be related to the solubility of its ideal state through its activity coefficient (Υ) which is given by expression (28) obtained by equating the activity a_c at the solution's equilibrium and that of its ideal state

$$\Upsilon = \frac{x_{ideal}}{x_e} \quad (28)$$

An activity coefficient equal to 1 indicates the solution behaves ideally i.e. the enthalpy of dissolution is equal to zero, as the energy needed to break solute-solute interactions added to that of breaking solvent-solvent interactions is equal to the energy released when solute-solvent bonds are formed. On the other hand, if activity coefficient is either lower or higher than 1 this would indicate a solution will dissolve more or less of the expected solute concentration at equilibrium respectively. For $\Upsilon > 1$ forces of attraction between like molecules would be favour over those of unlike molecules. For $\Upsilon < 1$ forces of attraction between unlike molecules would be favour over those of unlike molecules. Deviations from a solution's ideal behaviour can be due either to enthalpic or entropic factors and this can be established by comparing the solubility van't Hoff model line with that of the ideal solution under the same temperature range. If the slopes of the lines are different, dissolution would be both enthalpic and entropic driven. If the lines are parallel this would indicate that dissolution is only entropically driven.

3.3.2. Nucleation kinetics

Using the KBHR approach the analysis of nucleation kinetics, from polythermal experimental data, can be performed following the procedure in the flow chart given in Fig. 3 of the SI.

4. Results and discussion

4.1. Solubility

The average values for the collected crystallisation T_c and dissolution T_{diss} temperatures together with the corresponding standard deviations (SD) as a function of cooling rate q and concentration are presented in the SI. An example of the linear dependence of T_c and T_{diss} on q is given in Fig. 3. The saturation temperature T_e , obtained from the extrapolation to $0^\circ\text{C}/\text{min}$ of $T_{diss}(q)$ lines at each of the solution's concentrations, are also shown in Table 1 of the SI.

The specific data points used to model the solubility according to the van't Hoff equation are given in Table 2. together with the corresponding enthalpy and entropy of dissolution and mixing (ΔH_{mix}) and (ΔS_{mix}). The activity coefficients and their modelled dependence on temperature are also provided. Methyl stearate enthalpy (ΔH_m) and entropy of melting (ΔS_m) are $53.94 \left(\frac{\text{KJ}}{\text{mol}}\right)$ and $0.17 \left(\frac{\text{KJ}}{\text{mol K}}\right)$ respectively. The subtraction of these values from those of enthalpy and entropy of dissolution delivered the corresponding values of enthalpy and entropy of mixing. The comparative van't Hoff lines are given in Fig. 4.

van't Hoff plots fit well to a linear model for all solutions studied. This indicates consistency of structure of material, at the corresponding range of temperature. Activity coefficients are all higher than one indicating that solute-solute interactions are stronger in all cases. However, the significant lower values obtained in toluene together with the lowest enthalpy of mixing suggest that in these solutions solute-solvent interactions are stronger than in the other two solvent systems.

The highest solubility is observed in toluene and decreases as function of solvent in the following order: toluene > kerosene > dodecane. This is in the same order of polarity/aromaticity. Fatty acid methyl esters are organic compounds with medium polarity due to the presence in their chemical structure of both a COO-alkyl group and a non-polar long hydrocarbon chain. The solubility trend could be justified in terms of the solvent polarity and the like-dissolves-like rule of thumb i.e. a non-polar compound will be dissolved by non-polar solvents and vice versa. Straight chain n-alkanes such as dodecane with a dipole moment of around 0.07 D [40] are non-polar molecules which will have lower affinity with methyl stearate whose dipole moment calculated in vacuum ranges between 1.52 and 1.67 D. On the other hand toluene will show better affinity due to a higher dipole moment equal to 0.36 D [40]. Kerosene is expected to deliver solubility higher than that of dodecane but lower than that observed in toluene due to its composition that comprises different types of hydrocarbons molecules including aromatic species.

According to this, it could be expected that dipole-dipole interaction between methyl stearate and toluene molecules are stronger. Additionally, it has been hypothesised [40, 41] that the low activity coefficients obtained in the case of toluene are likely to be, to a great extent, due to the polarising effect created by the delocalised electron cloud around the benzene ring [41]. This could cause the distortion of the electron cloud around the solvent molecule inducing temporary dipoles among solute-solvent molecules which can be quite strong interactions in the case of the benzene ring, due to the effect of London dispersion forces [40]. This effect appears to be manifested through the very low ΔH_{mix} in toluene solvent, consistent with the high released of energy associated with the formation of these solute-solvent bonds.

The noticeable dependence of activities on temperature for kerosene solutions can be evidence on the steep slope of the van't Hoff line. Higher enthalpy and entropy of dissolution in this case are likely to be due to the range of different compounds present in kerosene, especially the aromatic molecules, which not only differ in size but will also complicate chemical interaction with the solute.

4.2. Nucleation kinetics

The relative critical undercooling u_c at the corresponding concentrations and cooling rates are presented in Table 1 of the SI. For each of the four solution concentrations within each solvent system a plot of cooling rate $q \left(\frac{K}{s} \right)$ vs. relative critical undercooling u_c in ln-ln coordinates was then constructed to obtain the slope of the straight line fitting these data points according to expressions (18 and 19).

Fig. 5 presents an example of the plot obtained for a concentration of 250 g/L in dodecane and kerosene solutions and for a concentration of 192 g/L in toluene solutions. The best linear fitting to these data is given by $y = 4.21 x + 13.41$, $y = 3.65 x + 10.76$ and $y = 7.16 x + 24.13$ respectively. The slope and the correlation coefficient R^2 of the best-fit straight line to the data for each concentration within the three solvent systems are presented in Table 3.

In all cases the slopes of the lines are higher than 3, suggesting that crystallisation of methyl stearate proceeds via the *PN* mechanism. Thus, according to the *KBHR* approach, equation (4) should describe the experimental data plotted in $\ln q$ vs. u_c coordinates. The values of a_1 , a_2 and $\ln q_0$ parameters obtained, using OriginPro 8.5.1., are presented in Table 3. For each

of the solution concentrations, within each solvent system these values along with the correlation coefficients for the fitting of equation (4) to the experimental are given.

The best-fit curves between the experimental $u_c(q)$ values and those calculated from equation (4) were obtained by setting $a_1 = 3$. An example of such a curve for the concentration of 250 g/l in dodecane and kerosene solutions and for a concentration of 192 g/l in toluene solution is presented in Fig. 6.

Even though a much lower range of cooling rates was used for the toluene solvent (0.25 to 1.5 °C/min compared to 0.25 to 9 °C/min for the other two solvents) the low values of R^2 , suggest that both relationships given by equations (4) and (18) are not followed. Thus, in this particular case further analysis could be undertaken by solving numerically equation (8) in the SM. The numerical solution of this equation would allow nucleation kinetic parameters to be obtained that would give a better fit regarding the dependence of the relative volume of crystals on the relative critical undercooling. Comparison of this trend line with the corresponding experimental data would provide an insight into whether this system can be better analysed using this more rigorous approach when compared to the constraints inherent in the analytical solution. In particular, such constraints describe only the early stages of crystallisation over which concentration can be assumed to remain virtually unchanged and hence the dependence of K_j and b on C and T can be effectively ignored. If this is the case the solution viscosity could also be assumed to remain virtually unchanged on cooling.

Nonetheless, the analysis was still performed for toluene solutions for comparison with the other two solvents.

According to equation (8) a_2 equals b , a dimensionless thermodynamic parameter defined by equation (10) from which the γ_{eff} can be calculated. The results obtained for $\ln q_0$ yield the values of q_0 , a parameter related through equation (9) to the nucleation rate constant K_j and the number N_{det} of crystallites at the detection point.

The effective interfacial tension γ_{eff} was evaluated from equation (10), using $v_o = 0.491 \text{ nm}^3$ [42], the calculated equilibrium temperatures T_e , the shape factor $k_n = \frac{16}{3}\pi$ for spherical nuclei and the molecular latent heat λ of crystallisation estimated to be 1.06×10^{-19} , 1.16×10^{-19} and $9.94 \times 10^{-20} \text{ J}$ for methyl stearate crystallising from dodecane, kerosene and toluene respectively. These values were calculated assuming the enthalpy of dissolution obtained from the solubility data can be equated to the enthalpy of crystallisation. In addition to this, the critical nucleus radius r^* and number i^* of molecules were obtained from equation (21) and (22) respectively, calculated at u_c levels obtained using T_c values corresponding to the extrapolation to $0^\circ\text{C}/\text{min}$ of $T_c(q)$ lines, at each of the four concentrations within each solvent system. The results are given in Table 4.

The low values of the effective interfacial tension are an indication of a prevalence of heterogeneous nucleation (*HEN*) mechanism for the nucleation of the methyl stearate crystallites regardless of the solution environment and are within the same order of magnitude of values reported earlier for n-alkanes [43-46].

The number of crystallites formed at the detection point N_{det} , at a given crystallisation temperature can be obtained by performing a mass balance using the van't Hoff models derived for each solvent system. Thus, using the corresponding values of mole fraction, the mass of C18:0 per unit volume in solution with the solvent can be obtained by solving the mass

parameter in the molar fraction relationship. The mass of C18:0 in the solid phase per unit volume is therefore the difference between the mass of C18:0 in the initial solution and the mass in solution at the corresponding crystallisation temperature. This value can be converted to volume by dividing the mass of the solute in the solid phase by the corresponding density.

Finally, the number of nuclei per unit volume i.e. N_{det} as a function of solvent and solution concentration can be estimated from dividing the total volume of solid by the volume of a single nucleus. The latter can be obtained using the values of the critical radius assuming spherical nuclei.

Following this, the nucleation rate constants K_J and nucleation rates J can be calculated from equation (9) and (23) respectively using $V = 1$, the corresponding equilibrium temperatures T_e , values of the dimensionless thermodynamic parameter b and values of the parameter q_0 for C18:0 as a function of solvent and concentration. A summary of these results is given in Table 4. The trend of these parameters is also shown in Fig. 4 of the SI.

Fig. 7 provides a comparison of the trend of nucleation rates (J) together with the critical radius (r^*) on an iso-supersaturation basis. r^* values were calculated using the interfacial tension obtained for each of the solutions' concentration studied at the corresponding σ levels.

4.2.1. Nucleation at the detection point

Nucleation rates are observed to be higher in kerosene where the supersaturation levels at which nucleation is detected are greater than in the other two solvents (Table 5.). The lowest values of the rates obtained for toluene solvent can be associated with the higher interfacial

tensions observed in this case, where the flatter nature of the slopes of the $T_c(q)$ lines show that nucleation proceeds more progressively or is a more thermodynamically controlled process. This is likely to be the result of the highest solubility of C18:0 in toluene which would favour solute-solvent interactions over solute-solute ones. In addition to this, in toluene systems the fraction (x_f) of methyl stearate that remains in solution at the corresponding crystallisation temperatures, are lower in comparison to those in the other two solvent systems (Table 4), as crystallisation occurs at lower temperatures in this case. Thus, given that interfacial tensions are inversely related to x_f , higher resistance to nucleation should be expected. In these solutions a sufficient level of supersaturation is then required to overcome the free energy for nucleus formation evidenced in the high levels of σ , which compares to those observed in kerosene where nucleation rates are at least one order of magnitude higher than in toluene.

Given that lower levels of interfacial tensions were observed in kerosene followed by dodecane solutions, it is likely that in these solvents nucleation is controlled, either by the attachment frequency f^* or the concentration of nucleation sites C_0 . This could indicate that either volume diffusion or interface transfer of building units (molecules) would be rate limiting according to expressions (24) and (25). In the case of kerosene solvent, these conclusions are in line with a higher range of σ at which higher x_f values were observed in comparison to dodecane solutions, allowing for both sufficient driving force nucleation and solute availability in solution that would reduce interfacial tension.

Interestingly, although similar values of interfacial tension to those of kerosene systems were obtained in dodecane solutions, the nucleation rates in the latter case were significantly lower by one order of magnitude. Given the expected lower strength of both solvent-solvent and

solvent-solute intermolecular interaction, due to the non-polar nature of dodecane molecules, the diffusion of solute molecules should not be rate limiting and therefore sufficient levels of attachment frequency should be possible to reach. Based on these observations and accounting for the definition of nucleation rate given by equation (23), it is likely that in these systems nucleation rates are then hindered by the availability of nucleation sites C_0 , due to the lower solubility of methyl stearate in dodecane that would allow a lower amount of solute per unit volume.

4.2.2. Nucleation at the same levels of supersaturation (σ)

If the analysis is performed comparing nucleation parameters at equal levels of solution supersaturation (Fig. 7), nucleation rates are higher in dodecane followed by kerosene and toluene solvent. The differences between dodecane and both kerosene and toluene solutions rates increase with an increase in σ up to even one order of magnitude at supersaturations higher than 80%. In general the critical nucleus radius is higher in toluene followed by kerosene and dodecane solutions, although this trend changes at the lowest and highest solution concentration studied in which kerosene solutions shows the highest and lowest values of this parameter respectively.

Given that the critical nucleus radius are directly related to interfacial tension, these observations confirm that interfacial tensions are rate limiting in toluene solvent over all the range of supersaturations chosen. Interfacial tensions in kerosene are closer in magnitude to those observed in dodecane solvent, while delivering nucleation rates closer in magnitude to those observed in toluene solutions. The latter complement the discussion presented in the previous section in the sense that this effect could be associated to the complex composition of

kerosene, which comprises molecules of different types including paraffins, cycloalkanes and aromatics, that could hinder the diffusion processes associated with molecular attachment into the nucleus and therefore decrease the attachment frequency (f^*).

Interfacial tensions were observed to be the highest in kerosene at the lowest solution concentration becoming closer to those observed in dodecane and below to those of toluene solutions as solutions concentration increases. This could be associated with an increase in the thermodynamic barrier to nucleation at lower concentrations where solute-solvent interactions would be favoured.

In the case of dodecane solutions the lowest values of interfacial tensions are in line with a more kinetically controlled process as discussed in section (4.2.1). The lower values of this parameter can be associated with the lower solubility of C18:0 in dodecane that favour solute-solute interactions. Likewise, attachment frequencies should be favoured by an easy de-solvation process due to the low solute-solvent strength interactions indicating that nucleation is likely to be hindered by the low values of C_0 .

The differences in the tendency observed when nucleation is analysed at the detection points in comparison to the same σ levels suggests that the complex composition of kerosene solvent significantly influence the nucleation process. In this case the role of thermodynamic and kinetics is more interconnected due to the different type of intermolecular interactions that would affect de-solvation and diffusion process as well as solubility.

A summary of the obtained solubility and nucleation kinetics parameters as well as some conclusions related to each section are given in Table 5.

5. CONCLUSIONS

The solubility and nucleation of methyl stearate crystallising from dodecane, kerosene and toluene was studied. Solutions of C18:0 in all cases show lower solubility than that of an ideal solution with the highest solubility obtained in toluene followed by kerosene and dodecane solvents. The analysis showed that in all cases a progressive nucleation mechanism and crystallite interfacial tension (γ_{eff}) values between 0.94-1.55, 1.21 - 1.52 and 1.18-1.88 $\frac{mJ}{m^2}$ for methyl stearate crystallising from dodecane, kerosene and toluene respectively. Nucleation rates calculated using the obtained values of γ_{eff} and the number of crystals at the detection point (N_{det}) ranged between 4.56×10^{16} and $1.79 \times 10^{17} \frac{nuclei}{mL \ sec}$, with the highest rates predicted for methyl stearate crystallising from kerosene solutions. This trend changes when the analysis is performed at the same σ levels where nucleation rates were the highest in dodecane solvent. This effect is thought to be due to the complex nature of kerosene in which the interplay between de-solvation, diffusion process and solubility plays a more important role.

ACKNOWLEDGEMENTS

The authors gratefully acknowledge Infineum Ltd. for the funding of this research which forms part of the doctoral studies of one of us (D.C.).

We also gratefully acknowledge the UK's EPSRC for the support of nucleation and crystal growth research at Leeds and Manchester through funding the Critical Mass Project: Molecules, Clusters and Crystals (Grant references EP/IO14446/1 and EP/IO13563/1).

The research on the analysis of nucleation data using the polythermal method was inspired by Professor Dimo Kashchiev (Institute of Physical Chemistry, Bulgarian Academy of Sciences) during his sabbatical leave in Leeds (Leverhulme Trust, Grant F10100A). We are most grateful to him for his insightful contribution to this research area.

LIST OF SYMBOLS

a Dimensionless molecular latent heat of crystallisation

a_c Solution activity

A^* Surface area of nucleus (m^2)

b Dimensionless thermodynamic parameter

C_{nuc}^* Equilibrium nucleus concentration (m^{-3})

C_0 Concentration of nucleation sites or instantaneously nucleated crystallites (m^{-3})

f^* Attachment frequency of monomers to the nucleus

J Nucleation rate ($m^{-3}s^{-1}$)

K_J Nucleation rate constant ($m^{-3}s^{-1}$)

k_n Nucleus numerical shape factor

n Crystallite growth exponent

N_{det} Detectable number of crystallites

q Cooling rate ($K s^{-1}$)

q_0 Parameter in the $u_c(q)$ dependence for both PN and IN ($K s^{-1}$)

Q Parameter in equation (10) related to q_0

T Solution temperature (K)

T_c Crystallisation temperature (K)

T_{diss} Equilibrium dissolution temperature (K)

T_e Solution saturation (or equilibrium) temperature (K)

ΔT_c Critical undercooling for crystallisation (K)

v_0 Volume of solute molecule in crystal (m^3)

V Volume of solution (m^3)

x Mole fraction of solute in solution

x_e Equilibrium mole fraction

x_{ideal} Ideal equilibrium mole fraction
 X_1 Concentration of colliding building units
 Z zeldovich factor
 ΔH_m Molal enthalpy of melting ($Jmol^{-1}$)
 ΔS_m Molal entropy of melting ($Jmol^{-1}K^{-1}$)
 ΔH_{diss} Molal enthalpy of dissolution ($Jmol^{-1}$)
 ΔS_{diss} Molal entropy of dissolution ($Jmol^{-1}K^{-1}$)
 ΔH_{mix} Molal enthalpy of mixing ($Jmol^{-1}$)
 ΔS_{mix} Molal entropy of mixing ($Jmol^{-1}K^{-1}$)
 i^* Number of molecules in critical nucleus
 r^* Critical nucleus radius (m)
 σ Relative supersaturation
 σ_{crit} Critical relative supersaturation
 u_c Relative critical undercooling for crystallisation
 Υ Activity coefficient
 γ_{eff} Effective interfacial tension of crystal nucleus in 3D HEN ($mJ m^{-2}$)
 λ Molecular latent heat of crystallisation (J)
 ρ Density
 ξ Sticking coefficient
 ω Positive number in expression (10)
 ω^* Transfer frequency of building units from adsorbed to integrated

LIST OF ABBREVIATIONS

HEN Heterogeneous nucleation

HON Homogeneous nucleation

IN Instantaneous nucleation

KBHR Kashchiev-Borissova-Hammond-Roberts approach

MSZW Metastable zone width

PN Progressive nucleation

SD Standard deviation

3D Three dimensional

Supplementary Information. Additional and more detailed materials are provided as a supplement to the paper including: comparative schemes for the isothermal or the polythermal method based on a concentration vs temperature profile, the full derivation of the set of expressions that comprise the *KBHR* approach , kerosene n-alkanes chain length distribution, temperature calibration lines for the Crystal 16 unit , flow chart describing how to apply the *KBHR* approach for the analysis of nucleation kinetics from polythermal experimental data, experimental crystallisation T_c and dissolution T_{diss} temperatures as a function of cooling rate q and comparative figures of nucleation kinetics parameters for methyl stearate crystallising from dodecane, kerosene and toluene solvents at the experimental crystallisation temperatures.

REFERENCES

- [1] D. Kashchiev, A. Borissova, R.B. Hammond, K.J. Roberts, Dependence of the critical undercooling for crystallization on the cooling rate, *J Phys Chem B*, 114 (2010) 5441-5446.
- [2] D. Kashchiev, A. Borissova, R.B. Hammond, K.J. Roberts, Effect of cooling rate on the critical undercooling for crystallization, *J Cryst Growth*, 312 (2010) 698-704.
- [3] D. Camacho, A. Borissova, R. Hammond, D. Kashchiev, K. Roberts, K. Lewtas, I. More, Nucleation mechanism and kinetics from the analysis of polythermal crystallisation data: methyl stearate from kerosene solutions, *Crystengcomm*, 16 (2014) 974-991.
- [4] M. Rubbo, J.N. Sherwood, An Improved Method for the Measurement of the Rates of Growth and Dissolution of Crystals Under Isothermal Conditions, *Journal of Crystal Growth*, 61 (1983) 210-214.
- [5] R. Boistelle, Calculation of the adsorption energies of n-alkane molecules on the (001) face of crystals of long-chain even n-alkanes, *Jornal of Crystal Growth*, 43 (1978) 141-147.
- [6] B. Simon, A. Grassi, R. Boistelle, Cinétique de Croissance de la Face (110) de la Paraffine $C_{36}H_{74}$ en Solution, *Journal of Crystal Growth*, 26 (1974) 77-89.
- [7] M. Rubbo, R. Boistelle, Dissolution and Growth-Kinetics of the (001) Faces of Normal-Hexatriacontane Crystals Grown from Heptane, *Journal of Crystal Growth*, 51 (1981) 480-488.
- [8] H.E. Lundagermadsen, R. Boistelle, Growth-Kinetics of the (001) Faces of Hexatriacontane ($C_{36}H_{74}$) in Solution, *Journal of Crystal Growth*, 46 (1979) 681-690.
- [9] W. Beckmann, R. Boistelle, Growth Kinetics of the (110) Face of Stearic Acid Growing from Butanone Solutions_Pure Solutions and in the Presence of an Emulsifier, *Journal of Crystal Growth*, 72 (1985) 621-630.

- [10] R. Boistelle, D. Aquilano, Interaction Energy and Growth Mechanisms on Twinned and Polytypic Crystals of Long-Chain Even Normal-Alkanes . I. Interaction-Energy Calculations, *Acta Crystallogr A*, 33 (1977) 642-648.
- [11] R. Boistelle, B. Simon, G. Pepe, Polytypic Structures of n-C₂₈H₅₈ (Octacosane) and n-C₃₆H₇₄ (Hexatriacontane), *Acta Crystallographica Section B-Structural Science*, 32 (1976) 1240-1243.
- [12] R. Boistelle, H.E.L. Madsen, Solubility of Long-Chain N-Alkanes in Petroleum Ether, *J Chem Eng Data*, 23 (1978) 28-29.
- [13] H.E. Lundagermadsen, R. Boistelle, Solubility of long-chain n-paraffins in pentane and heptane, *J. Chem. Soc., Faraday Trans. 1*, 72 (1976) 1078-1081.
- [14] H.E.L. Madsen, R. Boistelle, Solubility of Octacosane and Hexatriacontane in Different Normal-Alkane Solvents, *J Chem Soc Farad T 1*, 75 (1979) 1254-1258.
- [15] R. Boistelle, A. Doussoulin, Spiral Growth Mechanisms of (110) Faces of Octacosane Crystals in Solution, *Journal of Crystal Growth*, 33 (1976) 335-352.
- [16] N.U.S. Jr, V.P. Migo, K. Sato, M. Matsumura, Crystallization behavior of neat biodiesel and biodiesel treated with ozonized vegetable oil, *European Journal of Lipid Science and Technology*, 107 (2005) 689-696.
- [17] C. Boshui, S. Yuqiu, F. Jianhua, W. Jiu, W. Jiang, Effect of Cold Flow Improvers on Flow Properties of Soybean Biodiesel Biomass and Bioenergy 34 (2010) 1309-1313.
- [18] E. Odeigah, R.B. Janius, R. Yunus, Factors Affecting the Cold Flow Behaviour of Biodiesel and Methods for Improvement-A Review *Pertanika J. Sci. & Technolog.* , 20 (1) (2012) 1-14.
- [19] R.O. Dunn, M.W. Shockley, M.O. Bagby, Improving the Low Temperature Properties of Alternative Diesel Fuels: Vegetable Oil-Derived Methyl Esters *JAOCs*, 73 (1996) 1719-1728.

- [20] J.A.P. Coutinho, K. Knudsen, S.I. Andersen, E.H. Stenby, A local composition model for paraffinic solid solutions, *Chemical Engineering Science*, 51 (1996) 3273-3282.
- [21] J.A.P. Coutinho, F. Mirante, J. Pauly, A new predictive UNIQUAC for modeling of wax formation in hydrocarbon fluids, *Fluid Phase Equilibria*, 247 (2006) 8-17.
- [22] J.A.P. Coutinho, C. Dauphin, J.L. Daridon, Measurements and modelling of wax formation in diesel fuels, *Fuel*, 79 (2000) 607-616.
- [23] J. Pauly, J.L. Daridon, J.M. Sansot, J.A.P. Coutinho, The pressure effect on the wax formation in diesel fuel, *Fuel*, 82 (2003) 595-601.
- [24] J.C.A. Lopes, Et.al., Prediction of Cloud Points of Biodiesel, *Energy & Fuels*, 22 (2008) 747-752.
- [25] J.A.P. Coutinho, M. Gonc-alves, M.J. Pratas, M.L.S. Batista, V.F.S. Fernandes, J. Pauly, J.L. Daridon, Measurement and modeling of biodiesel cold-flow properties, *Energy & Fuels*, 24 (2010) 2667-2674.
- [26] J.M. Prausnitz, *Molecular thermodynamics of fluid-phase equilibria*, Prentice-Hall Inc., Englewood Cliffs N. J., 1969.
- [27] J.H. ter Horst, S. Jiang, Crystal nucleation rates from probability distributions of inductions times *Crystal Growth and Design*, 11 (2011) 256-261.
- [28] Y. Xiao, S.K. Tang, H. Hao, R. Davey, T. Vetter, Quantifying the inherent uncertainty associated with nucleation rates estimated from induction time data measured in small volumes, *Cryst Growth Des*, 17 (2017) 2852-2863.
- [29] J. Nyvlt, Kinetics of nucleation in solutions *J Cryst Growth*, 4 (1968) 377-383.
- [30] J. Nyvlt, R. Rychly, J. Gottfried, J. Wurzelova, Metastable Zone Width of some aqueous solutions *J Cryst Growth*, 6 (1970) 151-162.
- [31] N. Kubota, A new interpretation of metastable zone widths measured for unseeded solutions, *Journal of Crystal Growth*, 310 (2008) 629-634.

- [32] K. Sangwal, A novel self-consistent Nyvlt-like equation for metastable zone width determined by the polythermal method *Crystal Research and Technology*, 44 (2009) 231-247.
- [33] K. Sangwal, Recent developments in understanding of the metastable zone width of different solute-solvent systems *Journal of Crystal Growth*, 318 (2001) 103-109.
- [34] N.A. Mitchel, P.J. Frawley, Nucleation kinetics of paracetamol–ethanol solutions from metastable zone widths, *Jornal of Crystal Growth*, 312 (2010) 2740-2746.
- [35] D.G. Blackmond, Reaction progress kinetics analysis: a powerful methodology for mechanistic studies of complex catalytic reactions, *Angewandte Chemie-International Edition*, 44 (2005) 4302-4320.
- [36] D. Kashchiev, A. Firoozabadi, Induction time in crystallisation of gas hydrates, *Journal of Crystal Growth*, 250 (2003) 499-515.
- [37] D. Kashchiev, Nucleation basic theory with applications, in, Butterworth Heinemann, Oxford ; Boston, 2000.
- [38] D. Kashchiev, Nucleation: basic theory with applications, Butterworth-Heinemann, Oxford, 2000.
- [39] Q. Hussain, Crystallisation of long chain methyl esters in relation to their cold flow behaviour, in: School of Process Environmental and Materials Engineering, University of Leeds, Leeds, 2012.
- [40] J.J. Scheepers, E. Muzenda, M. Belaid, Influence of structure on fatty acid ester-alkane interactions, *International Conference on Chemical Engineering and its Applications*, (2012) 93-102.
- [41] J.J. Scheepers, E. Muzenda, M. Belaid, Influence of temperature and molecular structure on organics-biodiesel interactions using group contribution methods *Proceedings - World Congress on Engineering III* (2012).

- [42] C.H. MacGillavry, M. Wolthuis-Spuy, Crystal structure of an Orthorhombic Modification of Methyl Stearate, *Acta Crystallographica B26* (1970) 645-648.
- [43] D. Turnbull, R.L. Cormia, Kinetics of crystal nucleation in some normal alkanes liquids *The Journal of Chemical Physics*, 34 (1961) 820-831.
- [44] K.J. Roberts, J.N. Sherwood, A. Stewart, The Nucleation of n-Eicosane Crystals from Solutions in n-Dodecane in the Presence of Homologous Impurities, *Journal of Crystal Growth*, 102 (1990) 419-426.
- [45] A.R. Gerson, K.J. Roberts, J.N. Sherwood, An Instrument for the Examination of Nucleation from Solution and Its Application to the Study of Precipitation from Diesel Fuels and Solutions of Normal-Alkanes, *Powder Technol*, 65 (1991) 243-249.
- [46] B.D. Chen, L.J. Brecevic, J. Garside, Nucleation of tetracosane in hydrocarbon solvents, 12th symposium on industrial crystallisation, 2 (1993) session 4, 59-64.

Tables and Figures

Table 1. Composition of Kerosene from 2D Gas Chromatography analysis performed by Infineum UK

	Hydrocarbon	Mass %
Paraffins	unbranched alkanes	16.29
	Iso-paraffins	23.04
Cycloalkanes	Naphthenes	42.40
Aromatics	Alkyl Benzenes	7.60
	Benzocycloparaffins	6.80
	Naphthalenes	3.43
	Biphenyls/acenaphthenes	0.30
	Fluorenes	0.15

Table 2. Solubility, enthalpy and entropy of dissolution and mixing for methyl stearate in three different solvents, together with corresponding activity coefficients. Parameters values obtained by modelling solubility data according to the van't Hoff plot. (The errors of the slope and the intercept for enthalpy and entropy of dissolution refer to the 95% confidence interval)

Solvent	T (°C)	<i>molar fraction</i> (x_e)	ΔH_{diss} ($\frac{KJ}{mol}$)	ΔS_{diss} ($\frac{KJ}{mol K}$)	ΔH_{mix} ($\frac{KJ}{mol}$)	ΔS_{mix} ($\frac{KJ}{mol K}$)	γ 20 °C	$\ln \gamma = aT + b$
dodecane	18.70	0.132	63.55 ± 10.860	0.20 ± 0.037	9.61	0.03	2.01	$-0.013 T + 0.96$
	21.09	0.160						
	22.18	0.186						
	24.12	0.210						
Kerosene	17.25	0.123	69.80 ± 2.874	0.22 ± 0.098	15.87	0.05	1.85	$-0.022 T + 1.06$
	19.21	0.149						
	20.86	0.173						
	22.01	0.196						
Toluene	1.90	0.052	59.84 ± 3.785	0.19 ± 0.014	5.90	0.02	1.14	$-0.009 T + 0.31$
	4.36	0.064						
	6.04	0.076						
	7.50	0.088						

Table 3. Slopes of the best linear fit to data points in $\ln q$ vs. $\ln u_c$ coordinates and correlation coefficients; values of the free parameters a_1 , a_2 and $\ln q_0$ obtained from the data fitting in $\ln q$ vs. u_c coordinates according to equation (4) and correlation coefficients (the errors of the slope and the free parameters refer to the 95% confidence interval)

Con. (g/L)	Slope of $\ln u_c$ vs. $\ln q$	R^2 , linear fitting	Nucleation Mechanism	a_1	$a_2 = b$	$\ln q_0$	$q_0 \left(\frac{K}{s}\right)$	R^2 , fitting equation (4)
dodecane								
200	3.50	0.96	PN	3	$7.44 \times 10^{-5} \pm 4.15 \times 10^{-5}$	9.29 ± 0.26	10812.30	0.98
250	4.21	0.94	PN	3	$2.19 \times 10^{-4} \pm 8.71 \times 10^{-5}$	9.35 ± 0.37	11548.60	0.97
300	3.89	0.89	PN	3	$1.39 \times 10^{-4} \pm 1.09 \times 10^{-4}$	9.54 ± 0.60	13936.82	0.92
350	4.30	0.90	PN	3	$3.30 \times 10^{-4} \pm 1.69 \times 10^{-4}$	9.10 ± 0.55	8917.04	0.94
Kerosene								
200	4.92	0.95	PN	3	$5.21 \times 10^{-4} \pm 1.46 \times 10^{-4}$	8.98 ± 0.37	7967.05	0.97
250	3.65	0.94	PN	3	$1.32 \times 10^{-4} \pm 1.09 \times 10^{-4}$	8.64 ± 0.42	5639.21	0.95
300	4.22	0.99	PN	3	$2.62 \times 10^{-4} \pm 2.94 \times 10^{-5}$	8.70 ± 0.09	5998.83	0.99
350	3.92	0.95	PN	3	$2.39 \times 10^{-4} \pm 1.03 \times 10^{-4}$	8.67 ± 0.33	5847.80	0.97
Toluene								
154	3.98	0.56	PN	3	$1.76 \times 10^{-4} \pm 4.08 \times 10^{-4}$	7.94 ± 1.26	2815.71	0.57
192	7.16	0.94	PN	3	$6.83 \times 10^{-4} \pm 2.04 \times 10^{-4}$	9.59 ± 0.64	14662.96	0.94
231	6.65	0.54	PN	3	$7.09 \times 10^{-4} \pm 8.21 \times 10^{-4}$	9.38 ± 2.35	11823.57	0.55
269	6.42	0.79	PN	3	$5.32 \times 10^{-4} \pm 3.72 \times 10^{-4}$	9.38 ± 1.26	11852.21	0.78

Table 4. Nucleation kinetics parameters and nucleation rates for methyl stearate crystallising from three different solvents at four different solution concentrations. The critical radius, number of crystals at the detection point and nucleation rates are calculated at u_c corresponding to T_c values obtained by the extrapolation to $0^\circ\text{C}/\text{min}$ of $(T_c(q))$ lines x_e is the equilibrium solubility, u_c the relative critical undercooling, x_f is the fraction of methyl stearate that remains in solution at the corresponding crystallisation temperatures, σ is relative supersaturation, γ is interfacial tension, r^* is the critical nucleus radius, i^* is the number of molecules in the critical radius, N_{det} is the number of crystals at the detection point and J the nucleation rate

Solvent	$x_e \left(\frac{\text{mol solute}}{\text{mol solution}}\right)$	u_c	x_f	σ	$\gamma \left(\frac{\text{mJ}}{\text{m}^2}\right)$	$r^* (\text{nm})$	i^*	N_{det}	$J \left(\frac{\text{nuclei}}{\text{mL s}}\right)$
dodecane	0.132	0.010	0.10	0.32	0.94	0.84	5	2.43×10^{19}	6.70×10^{16}
	0.160	0.013	0.12	0.37	1.35	0.99	8	2.07×10^{19}	9.04×10^{16}
	0.186	0.011	0.13	0.38	1.16	0.98	8	2.57×10^{19}	1.06×10^{17}
	0.210	0.015	0.15	0.44	1.55	1.00	8	3.16×10^{19}	1.27×10^{17}
Kerosene	0.123	0.017	0.07	0.66	1.91	0.94	7	2.64×10^{19}	1.24×10^{17}
	0.149	0.014	0.10	0.50	1.21	0.74	4	5.83×10^{19}	1.48×10^{17}
	0.173	0.015	0.11	0.55	1.52	0.84	5	5.11×10^{19}	1.79×10^{17}
	0.196	0.015	0.13	0.54	1.48	0.85	5	5.47×10^{19}	1.68×10^{17}
Toluene	0.052	0.016	0.03	0.55	1.18	0.73	3	3.93×10^{19}	7.08×10^{16}
	0.064	0.016	0.04	0.49	1.86	1.17	14	1.08×10^{19}	4.56×10^{16}
	0.076	0.017	0.05	0.58	1.88	1.07	10	1.87×10^{19}	1.04×10^{17}
	0.088	0.015	0.06	0.49	1.71	1.13	12	1.64×10^{19}	6.53×10^{16}

Table 5. Summary of parameters obtained through the combined assessment of solubility, and nucleation kinetics of methyl stearate in three different solvents. γ is the activity coefficient, ΔH_{diss} and ΔS_{diss} are the enthalpy and entropy of dissolution respectively, ΔH_{mix} and ΔS_{mix} are the enthalpy and entropy of mixing respectively, γ is the interfacial tension, r^* is the nucleus critical radius and J is the nucleation rate

Assessed criteria	Assessed parameters	Dodecane	Kerosene	Toluene	Conclusion
Solubility	Solubility level	Lowest	Intermediate	Higher	All systems behave less than ideal as activities are higher than one. However, higher values in dodecane followed by kerosene solutions indicate either solute-solute or solvent-solvent interactions are favoured in these systems. Solute-solvent interactions are similar to those of solute-solute in toluene solutions as activities close to 1, this is further supported by the lowest enthalpy of mixing. The highest values of both enthalpy of dissolution and mixing in kerosene solution evidence strong dependence of activities on temperature.
	γ (20°C)	2.01	1.85	1.14	
	ΔH_{diss} ($\frac{KJ}{mol}$)	63.55	69.81	59.84	
	ΔS_{diss} ($\frac{KJ}{mol K}$)	0.20	0.22	0.19	
	ΔH_{mix} ($\frac{KJ}{mol}$)	9.61	15.87	5.90	
	ΔS_{mix} ($\frac{KJ}{mol K}$)	0.03	0.05	0.02	
Nucleation	Range σ	0.32-0.44	0.50-0.66	0.49-0.58	Relatively higher values of interfacial tensions in toluene seem to hinder nucleation in this solvent. Although interfacial tension values are close in dodecane and kerosene solutions, nucleation in the former is one order of magnitude lower. This could indicate less available nucleation sites in these solutions, due to the low solubility of methyl stearate in dodecane.
	Range γ ($\frac{mJ}{m^2}$)	0.94-1.55	1.21-1.52	1.18-1.88	
	Range r^* (nm)	0.84-1.00	0.74-0.94	0.73-1.17	
	Range J ($\frac{nuclei}{mL s}$)	$6.70 \times 10^{16} - 1.27 \times 10^{17}$	$(1.24 - 1.79) \times 10^{17}$	$4.56 \times 10^{16} - 1.04 \times 10^{17}$	

*These results are presented together with those obtained for the assessment of morphology and crystal growth kinetics, for the same solutions' systems, in Camacho D.M. et al., Morphology and Growth of methyl stearate as a function of crystallisation environment, Cryst. Growth Des., (2017), 17, 563-575

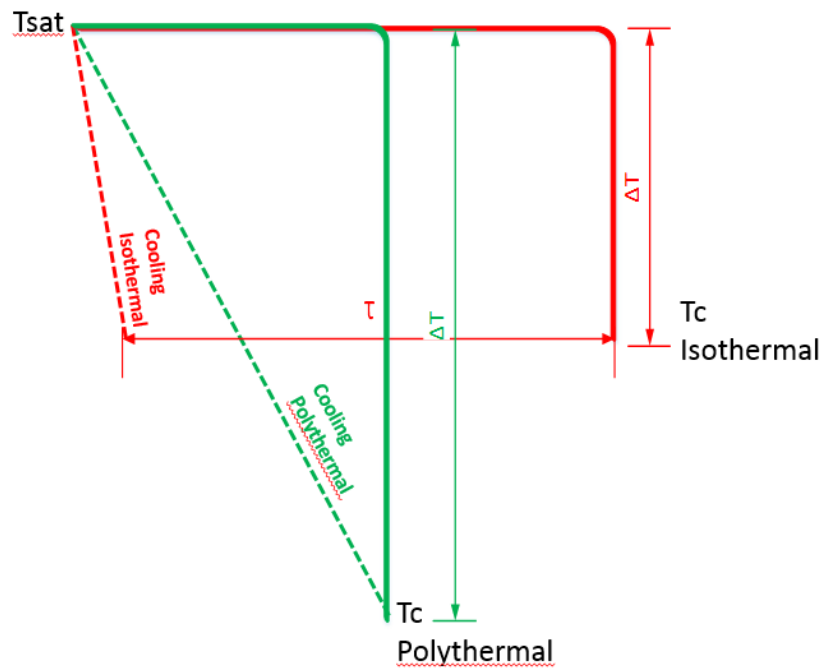


Fig. 1 Comparative scheme of the different approaches used to collect experimental crystallisation temperatures using both the isothermal and the polythermal methods

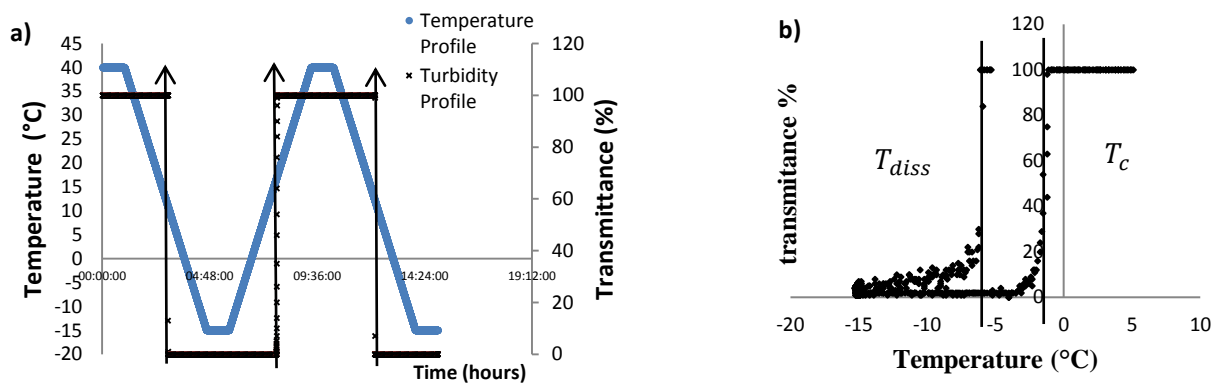


Fig. 2 a) Typical experimental profile using Crystal 16® by applying the polythermal method. b) Representative turbidity profile in transmittance vs. temperature coordinates obtained by the application of a polythermal method

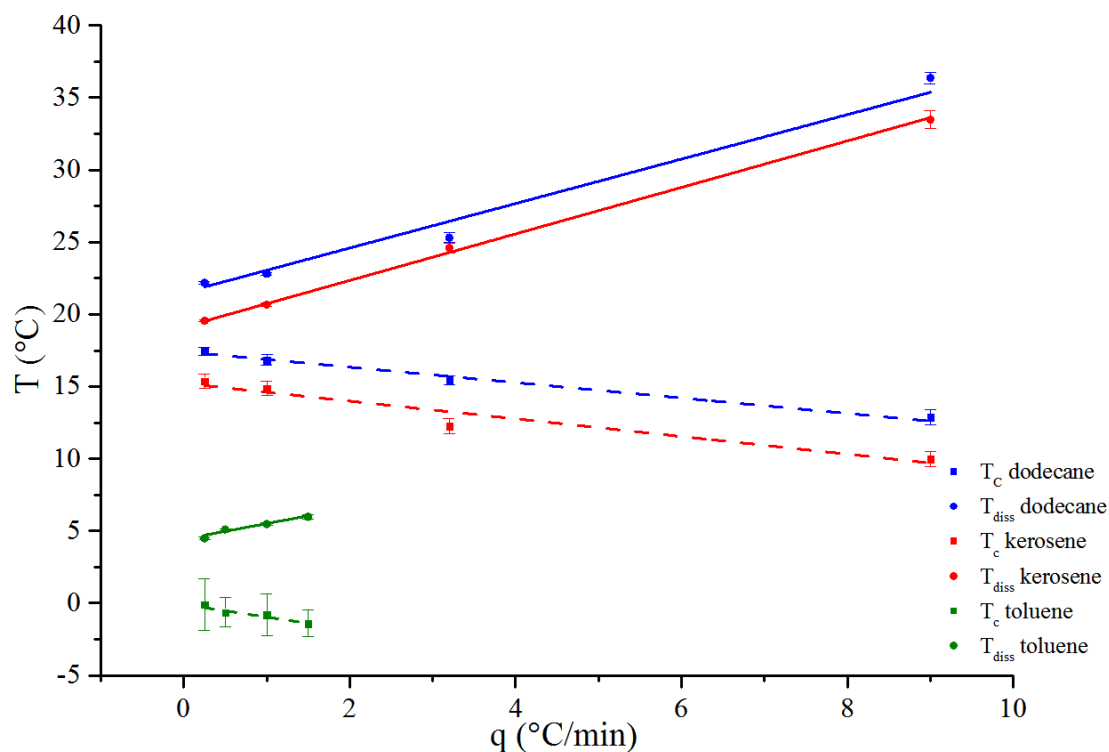


Fig. 3 Crystallisation T_c and dissolution T_{diss} temperatures as a function of cooling rate q for solution concentrations of 250 g/L for methyl stearate crystallising from dodecane and kerosene solvents and of 192 g/L for methyl stearate crystallising from toluene solvent

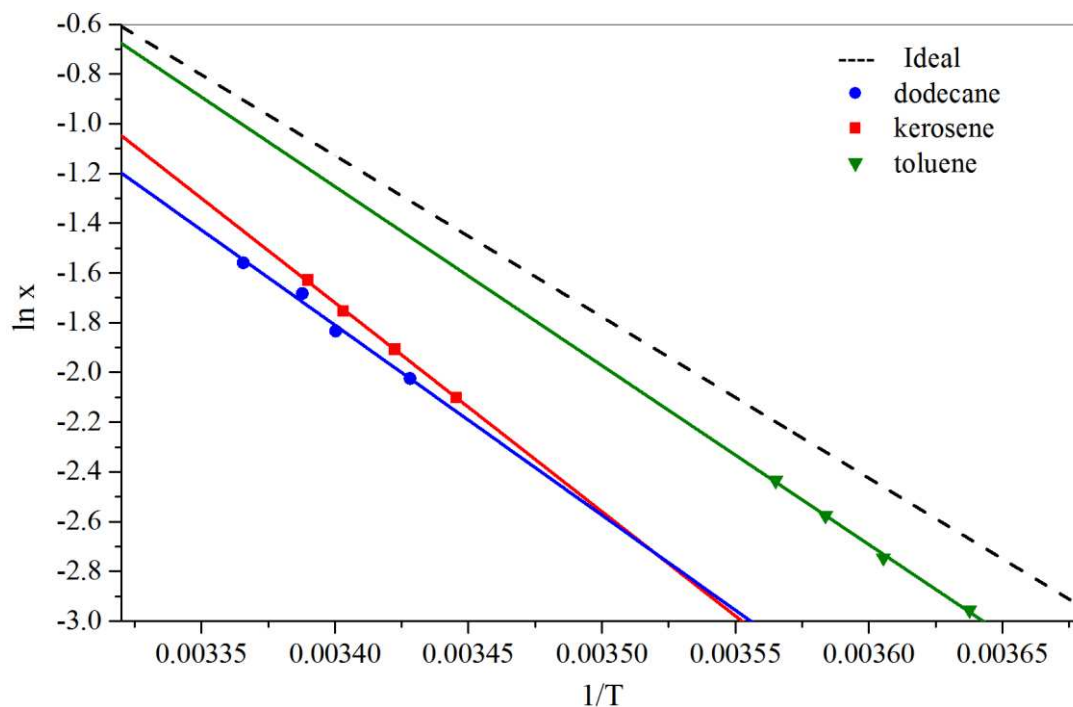


Fig. 4 van't Hoff plot for methyl stearate in three different diesel type solvents. Solid lines represent experimental solubilities and the dashed line the ideal solubility. Experimental solubilities were obtained by extrapolation to 0°C of $T_{diss}(q)$ lines at four different solution's concentrations

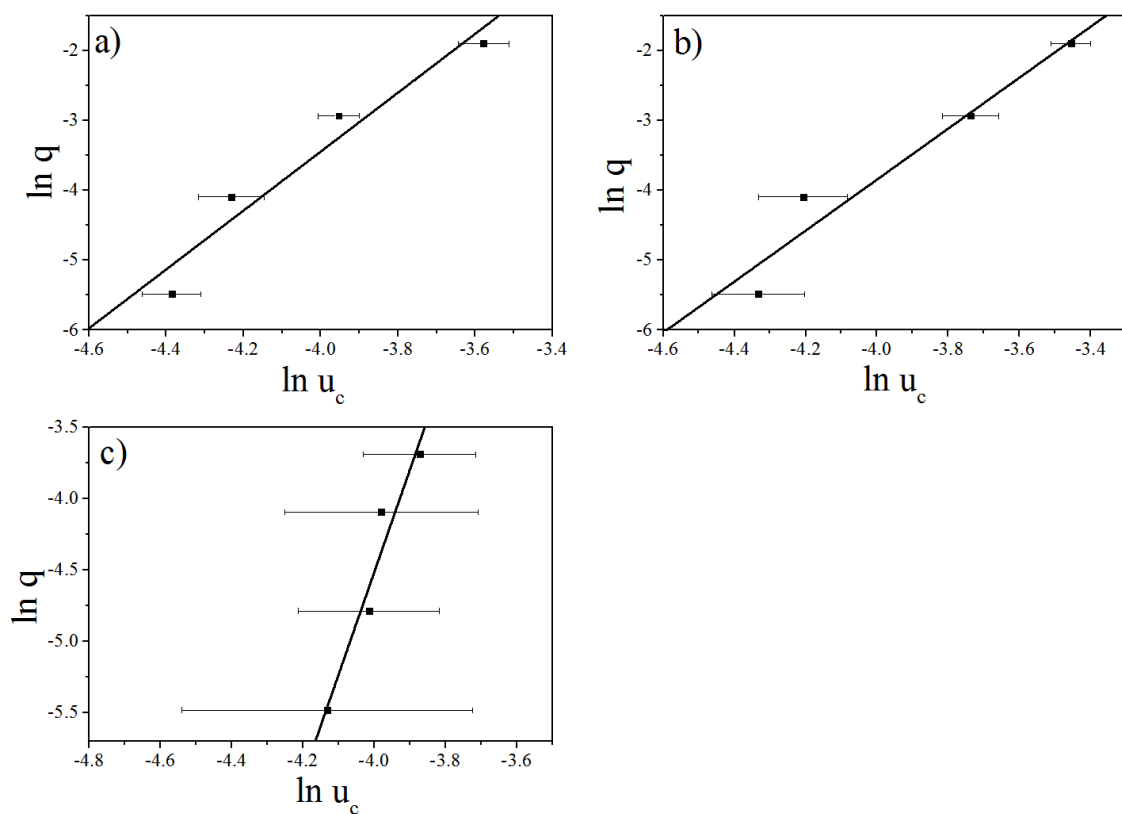


Fig. 5 Experimental polythermal data in $\ln q$ vs $\ln u_c$ coordinates for solution concentrations of 250 g/L and 192 g/L for methyl stearate crystallising from a) dodecane and b) kerosene solvents and c) for methyl stearate crystallising from toluene solvent respectively

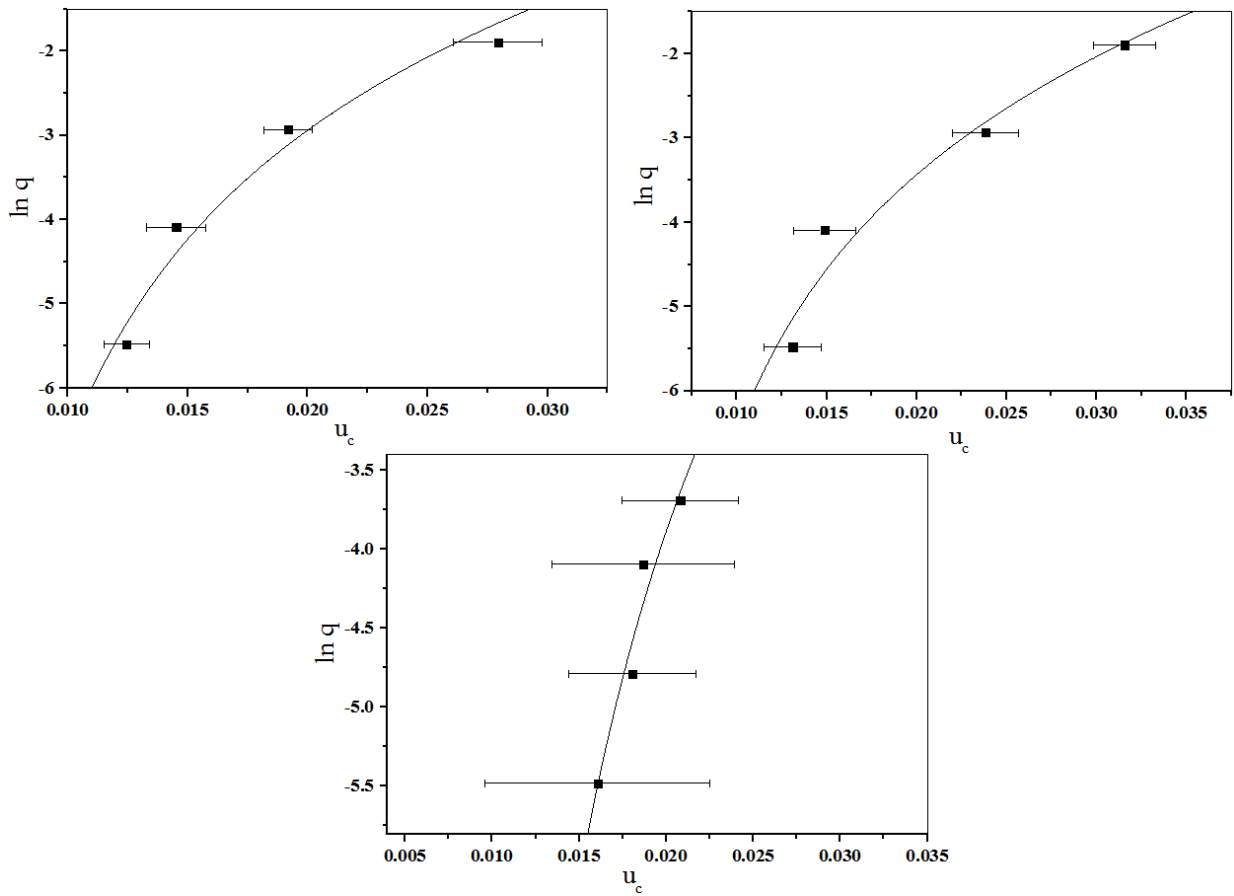


Fig. 6 Increase in relative critical undercooling with the natural logarithm of cooling rate. The points represent the data for crystallisation of methyl stearate in solution with a) dodecane 250 g/L b) kerosene 250 g/L and c) toluene 192 g/L; the line illustrates the best fit according to equation (4)

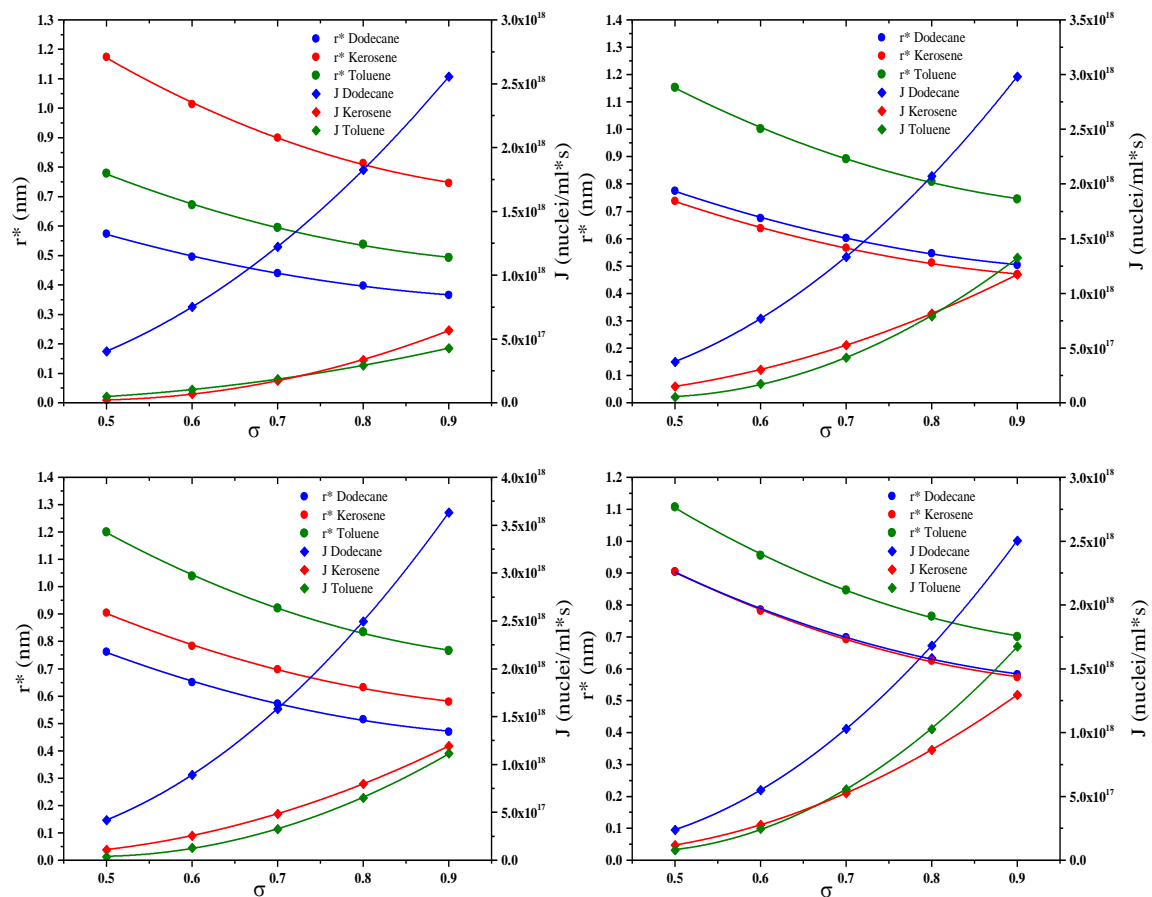


Fig. 7 Tendency of critical radius (r^*) and nucleation rates (J) as a function of supersaturation (σ) for C18:0 growing from dodecane, kerosene and toluene solvents using parameters derived for the range of concentrations studied. Concentration increases from left to right and from top to bottom